A new pneumatic pad controlled by means of an integrated proportional valve

AIMETA 2019
XXIV Conference
The Italian Association of Theoretical and Applied Mechanics
Rome, Italy, 15-19 September 2019

A NEW PNEUMATIC PAD CONTROLLED BY MEANS OF AN INTEGRATED PROPORTIONAL VALVE

F. Colombo[1], **D. Maffiodo**[1], **and T. Raparelli**[1]

[1] Department of Mechanical and Aerospace Engineering, Politecnico di Torino
e-mail: {federico.colombo, daniela.maffiodo, terenziano.raparelli}@polito.it

Keywords: aerostatic pad, active compensation, proportional valve.

Abstract. *Aerostatic air bearings have the advantages of supporting loads with no friction and wear and for this feature they are extensively adopted in metrology as they allow very precise motion. The possibility of integrating an active component increases the performance of the aerostatic pads, which can be designed in order to obtain an infinite stiffness or to improve stability. In [1,2] the authors developed a prototype of active pad controlled by means of digital valves and Arduino board. A shortcoming of this prototype was a small amplitude oscillation of the pad supply pressure due to the opening and closing of the digital valve. In order to overcome this problem a new prototype was designed making use of a proportional valve. This paper shows the first experimental tests together with the numerical model.*

1 INTRODUCTION

Pneumatic thrust bearings are used for precision positioning and in measuring machines thanks to their main feature: the very low friction. Depending on the application, the characteristic of having a reduced stiffness, and therefore a high sensitivity to the load, may represent an important limit for the correct operation of the device, as generally happens in measurement systems.

Various researches have been carried out investigating on passive or active solutions to increase the rigidity of the thrust bearing. The passive type systems [1-4] generally work well only around a predetermined operating point and have low bandwidth.

As for pads with active systems, they allow to reach higher bandwidth even if they are generally more complex and with a greater number of components.

In the literature there are examples of active thrust bearings that exploit different operating principles: from magneto-strictive elements [5] to magnetic preload actuators [6], from piezoelectric elements [7, 8] to pneumatic valves [9-11]. A literature review on the solutions proposed by researchers is available in [12].

None of these devices is currently used in the industrial field and the present challenge consists in the realization of a device that not only has good operating characteristics, but also low costs, for real use.

The authors have already worked on a previous low cost device and embedded components [13-15] with digital pneumatic valves.

The new prototype of an active pneumatic pad presented in this paper arises from the considerations made after the previous work. In this first prototype, a commercial pneumatic pad has been assembled with sensors detecting the height of air gap under the pad and with two digital pneumatic valves for air supply and discharge of the pad. The air gap measurement was compared with a set value and the duty cycle of the PWM which controls the opening and closing of the digital valves was consequently modified. The results of this first prototype are encouraging in terms of response of the system to variations in load on the pad. However, the oscillations due to the opening and closing of the digital valves cannot be avoided.

The proposed new solution uses a flow proportional pneumatic valve in place of the two digital electro pneumatic valves.

2 THE NEW PROTOTYPE OF PNEUMATIC PAD

Figure 1 shows the photo of the new prototype, while Figure 2 sketches its pneumatic circuit. The passive pad (1) is actuated by a proportional electro-pneumatic valve SMC PVQ10 (2) which is controlled by a current signal from an electronic board (3). The air gap under the pad h is measured by two back pressure sensors (5) properly designed connected to pressure transducers Honeywell 40PC (4). The signal from these sensors is fed back to the controller in case of closed loop operation.

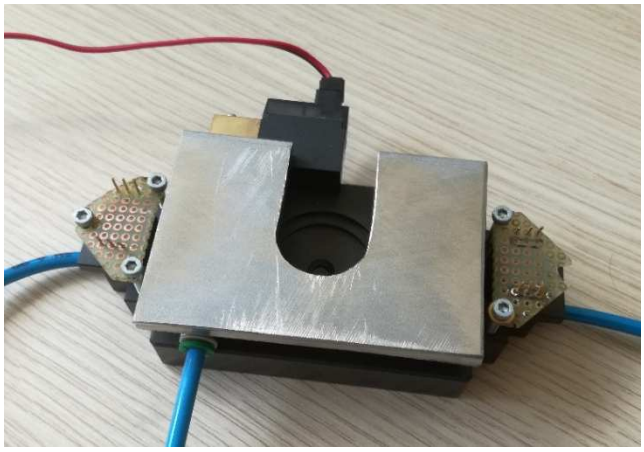

Figure 1: Photo of the prototype

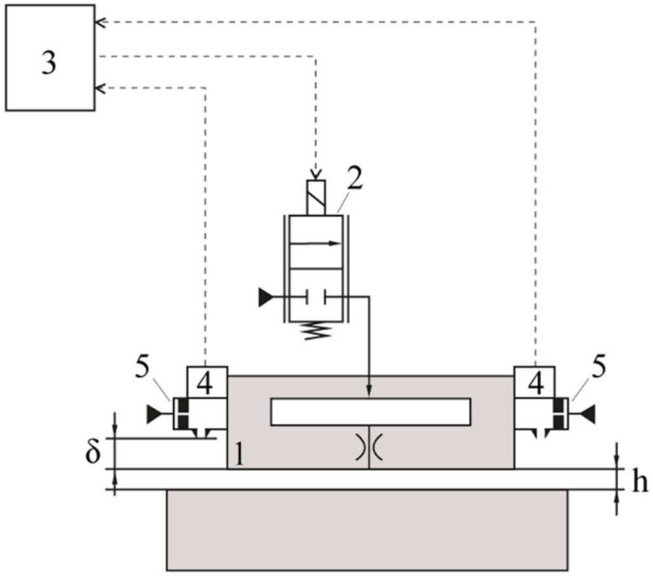

Figure 2: Functional scheme of the device; pad (1), proportional pneumatic valve (2), electronic board (3), pressure transducers (4), backpressure sensors (5), height of the air film (h), backpressure sensor offset (δ)

The SMC PVQ10 valve (Figure 3) is a small size pure proportional pneumatic solenoid valve. The output air flow is proportional to the current input signal. The valve is normally closed and the sleeve is kept in position with the use of a spring, see Figure 3a. To connect the valve to the pad an interface block is needed, see Figure 3b.

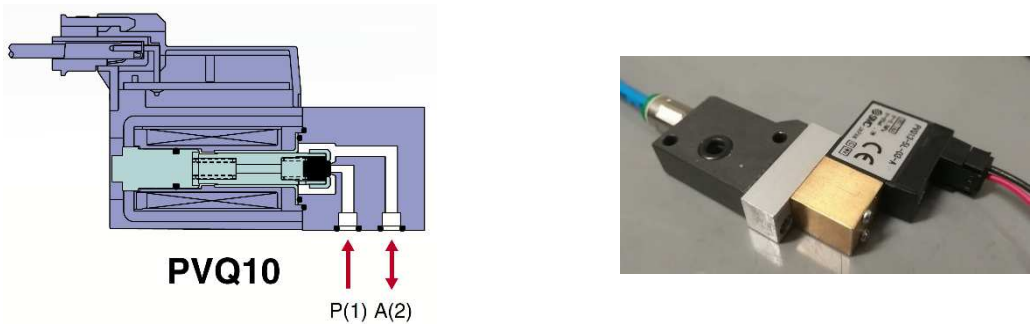

(a) (b)

Figure 3: SMC PVQ10 proportional valve (a) internal section (b) picture of the valve with interface block

When the valve is energised, the current flows through the solenoid which creates a magnetic force on the sleeve and, when this force overcomes the spring force, lifts the sleeve allowing the air to flow through. The higher the current flowing through the coil, the greater will be the stroke of the armature and the air flow. The equivalent orifice diameter of the valve is 0.3 mm able to be crossed by an airflow up to 4 l/min ANR with a maximum gauge supply pressure of 0.7 MPa. The valve needs to be current controlled in range 0-85 mA with a voltage up to 24 VDC. At this purpose, a current drive circuit has been designed to convert the voltage coming from the electronic board into a proportional current flowing through the solenoid of the valve.

2.1 Experimental characterization of the valve

Preliminary tests have been carried out on the valve in order to evaluate the start-up current, the hysteresis cycle of the valve and its dynamic parameters, natural frequency and damping.

The first quasi-static test is carried out in two different configurations: i) the valve without the pad, connected with the interface block; ii) the valve with interface block assembled on the pad. Each test was performed with gauge supply pressure equal to 0.5 and 0.7 MPa.

A triangular wave current centered at 60 mA and with an amplitude of 30 mA was applied to the valve, with a very low frequency (0.1 Hz). The flow through the valve was measured by a digital flow meter. As shown in Figure 4, a small hysteresis is present, mostly due to the friction in the prismatic coupling between the moving sleeve and the valve body where an O-ring prevents flow leakage.

It can be noticed that the valve has a dead band which is dependent on the supply pressure. Increasing the supply pressure, the dead band reduces as the supply pressure works opening the valve internal anchor.

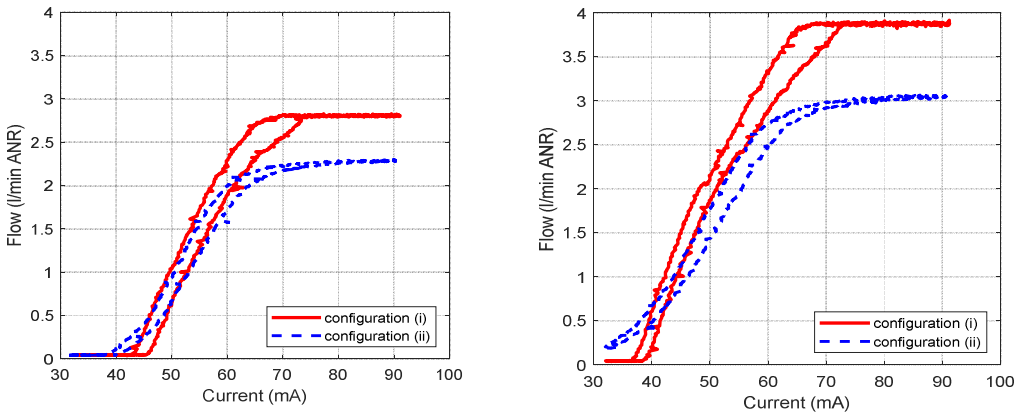

Figure 4: Valve characteristics at (a) 0.5 MPa gauge supply pressure and (b) 0.7 MPa

The two configurations present different values of maximum air flow because in configuration (ii) the presence of the thrust bearing represents an additional pneumatic resistance of the circuit. Moreover, this resistance is causing also the need for a higher current (80 mA) to obtain the maximum flow in configuration (ii) than in configuration (i) (75 mA).

The start-up current values are different in the two configurations and for the different supply pressures. In fact, according to the working principle of the pneumatic valve, the opening to let the air flow through the valve is controlled by the equilibrium of the moving sleeve between the spring and the magnetic force generated by the coil, but depends also on the pressure values at the inlet and outlet port of the valve. The higher the supply pressure to the valve, the lower

the current needed to open the sleeve. The outlet pressure helps the opening of the valve too. This explains why the start-up current values are different for configuration (i) and (ii) when the same pressure supply is present. As explained before, the bearing introduces a pneumatic resistance between the valve and the ambient pressure at its outlet hole. For configuration (i) outlet pressure is ambient pressure, for configuration (ii) the outlet pressure of the valve is higher than the ambient pressure and facilitates the opening of the valve.

The dynamic behavior of the valve, tested in configuration (i) has been analyzed by means of a series of sinusoidal current input signals of increasing frequency. Signal amplitude is 10 mA, ranging from 65 mA to 75 mA, for all the tests. Frequency range is from 1 Hz to 100 Hz. The measured output was the flow through the valve. Comparing the results of each test with the static results, it was then possible to obtain the dimensionless Bode diagram shown in Figure 5.

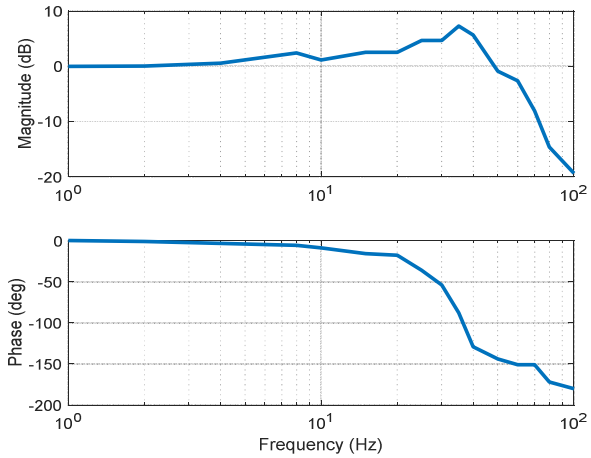

Figure 5: Bode plot of the pneumatic valve

The natural frequency of the valve is about 35 Hz. When the frequency is greater than 50 Hz the amplitude of the oscillations of the output is under the value of 0 dB and with frequency higher than 70 Hz the oscillations hardly follow the sinusoidal input.

In order to experimentally determine the damping of the valve, a step test was carried out. With a gauge supply pressure of 0.5 MPa, a step current signal from 0 mA to 60 mA was given to the valve and the flow through the valve was acquired. The experimental results are shown in Figure 6 (dotted blue line). Since the pneumatic valve can be approximated with a second order system with natural frequency ω_n and damping factor ζ, the transfer function of the pneumatic valve H(s) with the current as input and the air flow as output is given by

$$H(s) = \frac{K_Q \omega_n^2}{s^2 + 2\zeta\omega_n s + \omega_n^2} \tag{1}$$

where ω_n is the valve natural frequency, ζ is the valve damping factor and K_Q is the static gain between current and air flow. Figure 6 shows the simulated step response with ω_n=35 Hz and ζ= 0.2 (in red solid line) and the experimental results from the experimental test on the pneumatic valve (in blue dotted line). The two curves have similar logarithmic decrement. Some non-linear effects due to friction between the sleeve and the valve body were not taken into account in the model. The Bode plot of the simulated second order system has been drawn and compared with the one obtained from the experimental tests. Since also the Bode plots are in good accordance, the second order transfer function (1) was used in the model.

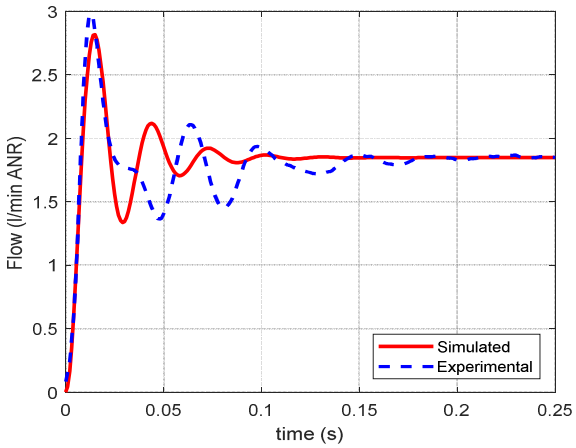

Figure 6: 60mA step test response, air flow through the valve for experimental test (dotted blue line) and simulation (red solid line)

2.2 Static tests on the active pad in open loop

A test bench has been set up in order to measure the static characteristics of the pad in passive and active configurations as depicted in Figure 7.

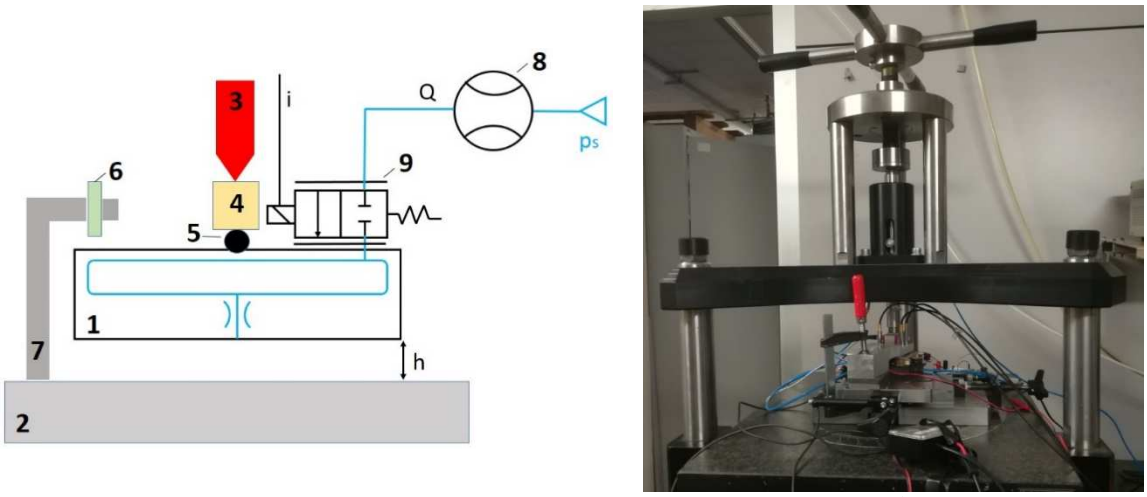

(a) (b)

Figure 7: Static test bench (a) sketch (b) picture

Pad (1) is laying on a steel plate (2). A vertical load (3) is established on the pad by means of a lead screw arrangement and a load cell FUTEK LRF350 (4) measures the force applied. Between the load cell and the bearing, there is a steel sphere (5) used to automatically align the generated force to the vertical axis. Four capacitive sensors Micro-epsilon capaNCDT (6) are used to measure the vertical displacement of the pad and compare it with the signal from the back pressure sensors. The capacitive sensors are fixed on a sensor holder (7) and they face the pad top surface near the four edges (see legend of Figure 7). The air flow is measured with a digital flowmeter Festo SFAB (8) placed before the inlet of the pneumatic valve (9).

Preliminar tests were performed at constant input current. Figure 7 shows an example at gauge supply pressure p_s=0.7 MPa and with the valve open at 75% of the maximum stroke.

The test procedure was the following: a) proportional valve completely closed and load force on the thrust bearing set to about 500 N; b) set of a constant input current causing the sleeve to

move of a given stroke; c) quasi static decreasing of the applied force; d) closing of the valve; e) increasing of the force to the starting value. Signals from load cell, capacitive sensors and flowmeter are acquired during the whole test execution.

As an example, Figure 8 shows the static curves at 0.7 MPa gauge supply pressure and valve opening of 75%. Plots represent the force applied on the pad (a) and the air flow (b) as a function of air gap height.

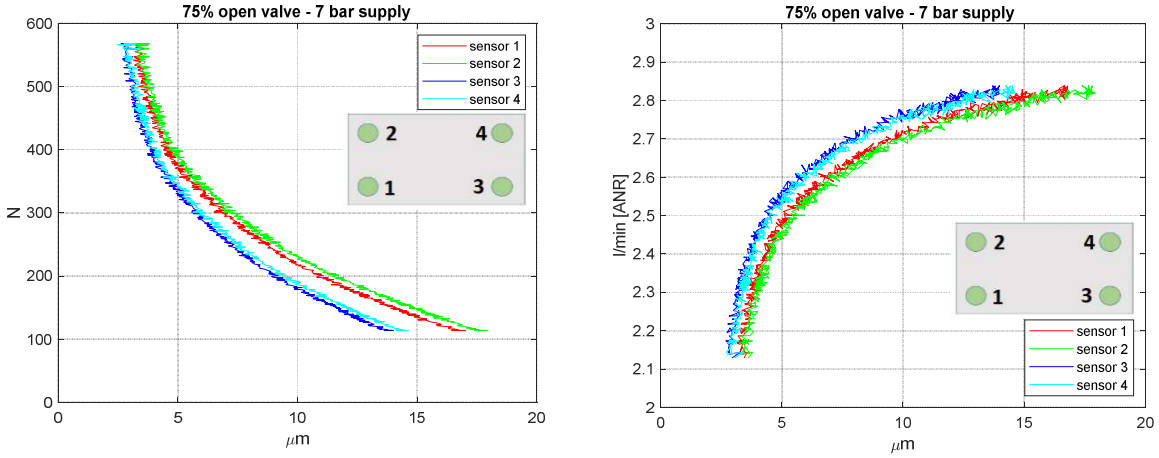

(a) (b)

Figure 8: Test results with gauge supply pressure 0.7 MPa; valve opening 75% (a) Force and (b) air flow vs air gap height

It can be noticed that the bearing shows a small tilting around a bearing axis as the sensors do not measure the same displacement. Sensors 1 and 2 on the left detect a slightly higher displacement than sensors 3 and 4 on the right.

3 THE NUMERICAL MODEL

3.1 Static model of the pad

The pad is composed of two resistances in series located in correspondence of the supply orifice (R_p) and inside the air gap (R_h) respectively. Among these, the capacitance C_p of the air gap is considered.

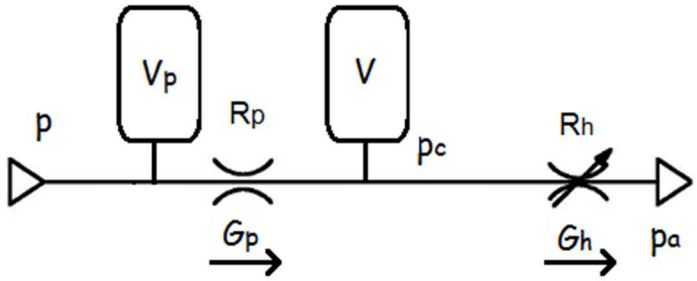

Figure 9: Sketch of the pneumatic circuit representing the pad

In static conditions, the air gap is imposed, while the load capacity and the air consumption are calculated in output.

3.1.1. Supply orifice model

Air flow in sonic conditions (P_c<bP):

$$G_p = \frac{\pi d_s^2}{4} \psi c_d P \tag{2}$$

where b is the critical ratio, P the absolute supply pressure of the pad and P_c the absolute pressure downstream the supply orifice. c_d is the discharge coefficient of the supply orifice, considered a function of the air gap h and the diameter d_s of the orifice:

$$c_d = 0.85\left(1 - e^{-8.2\frac{h}{d_s}}\right) \tag{3}$$

Air flow in subsonic conditions (bP<P_c<P):

$$G_p = \frac{\pi d_s^2}{4} \psi c_d P \sqrt{1 - \left(\frac{\frac{P_c}{P} - b}{1 - b}\right)^2} \tag{4}$$

3.1.2. Model of the air gap

The air film is modeled as a lumped capacitance C_p and a lumped resistance R_h. Capacitance C_p is related to the air volume V under the pad by

$$C_p = \frac{V}{RT} \tag{5}$$

under the hypothesis of isothermal conditions, where R is the gas constant and T the absolute temperature. The volume is proportional to the gap height h and to the pad surface S: V=Sh. The resistance of the air gap is inversely proportional to the air gap:

$$R_h = \frac{1}{c_h h^3} \tag{6}$$

where c_h is a coefficient that can be calculated for each pad geometry. So the air flow G_h through the gap is given by

$$G_h = \frac{P_c^2 - P_a^2}{R_h} \tag{7}$$

where P_a is the ambient pressure (absolute).
The continuity equation written in dynamic conditions for volume V in case of constant air gap is

$$G_p - G_h = \frac{Sh}{RT} \dot{P}_m \tag{8}$$

where P_m denotes the mean pressure under the pad. This value is related to the supply holes downstream pressure P_c, which is the maximum pressure under the pad. It was found that a linear function like the above is of good approximation, where k is a constant typical of each pad:

$$P_m - P_a = k(P_c - p_a) \tag{9}$$

The load capacity is given by

$$F_c = (P_m - P_a)S \tag{10}$$

For the pad under study, the following values were used: c_h=0.8 s/m^2 and k=1/3.
Figure 10 shows the static characteristics of load capacity and air flow consumption of the pad in passive operation, that is directly connected to the supply (without valve).

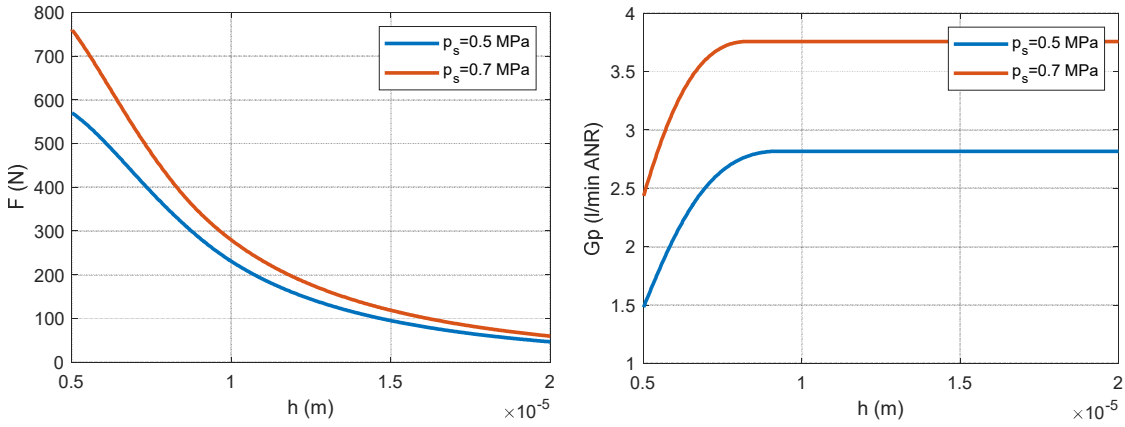

Figure 10: Pad static curves at p_s=0.5 and 0.7 MPa (gauge) in passive operation (without valve)

3.2 Dynamic model of the pad

In dynamic conditions, the external force on the pad F is imposed, while the air gap results from the vertical equilibrium of forces:

$$F + (m + M)\ddot{h} - F_c = 0 \tag{11}$$

where m is the pad mass and M is the mass of the supported structure. The weight of the supported structure (M=10 kg) and the external force F are considered separately to be able to simulate a general preloading condition, like e.g. magnetic preloading.
The continuity equation written in dynamic conditions for volume V is

$$G_p - G_h = \frac{S}{RT}\left(P_m\dot{h} + h\dot{P}_m\right) \tag{12}$$

Figure 11 shows the response to an external force step from 150 N to 200 N. The air gap decreases from about 12 µm to 11 µm. The integral of the pressure distribution F_c in static conditions equals the external force F.

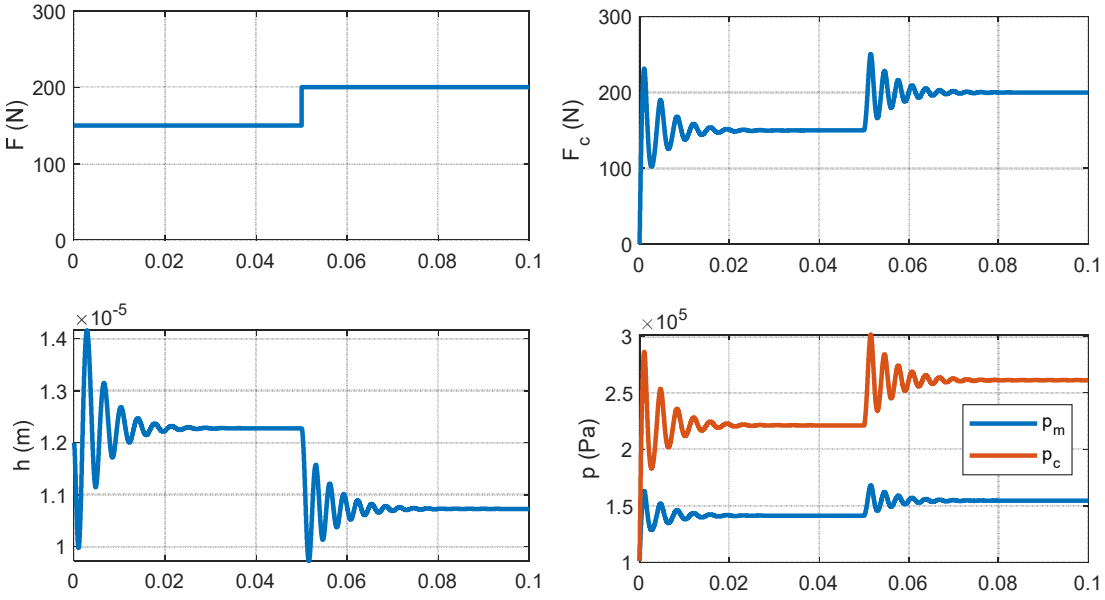

Figure 11: Response of the pad to a positive external force step with p_s=0.5 MPa (gauge)

The transient expires after a time interval of about 0.02 s due to the damping capacity of the air gap. In case the reaction force F_c is plotted vs the air gap h (see Figure 12), it can be seen that the force is not proportional to the air gap but it is delayed due to damping. In this case every cycle is associated to an energy dissipation as damping is positive; in case of negative damping, the cycle is traversed in opposite direction.

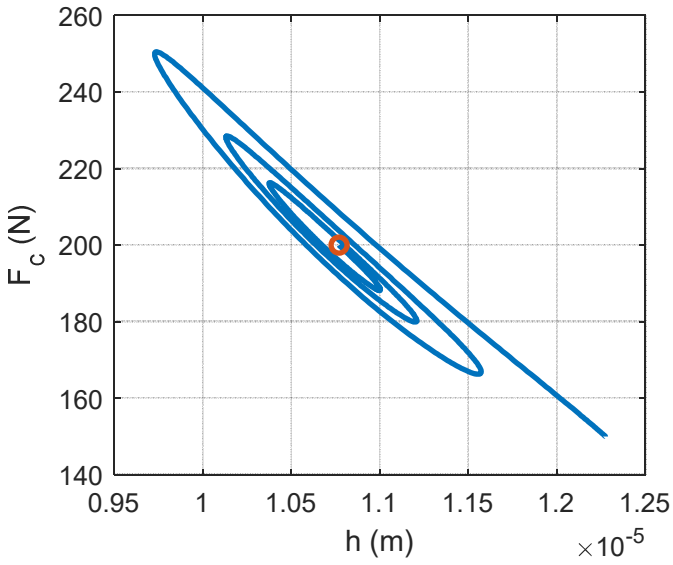

Figure 12: Phase diagram between the pad load capacity and the air gap in dynamic conditions

3.3 Model of the proportional valve

3.3.1. Static model of the valve

The valve conductance is a function of the input current; the linear approximation is given by $C_{st} = K_v i$, where K_v is the static gain between current and air flow, while a non-linear relationship can be defined by function $C_{st}(i)$.

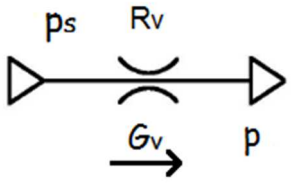

Figure 13: Sketch of the valve pneumatic circuit

With this relationship it is possible to take into account the dead-band at small values of current. The dead band amplitude changes depending on the supply pressure.

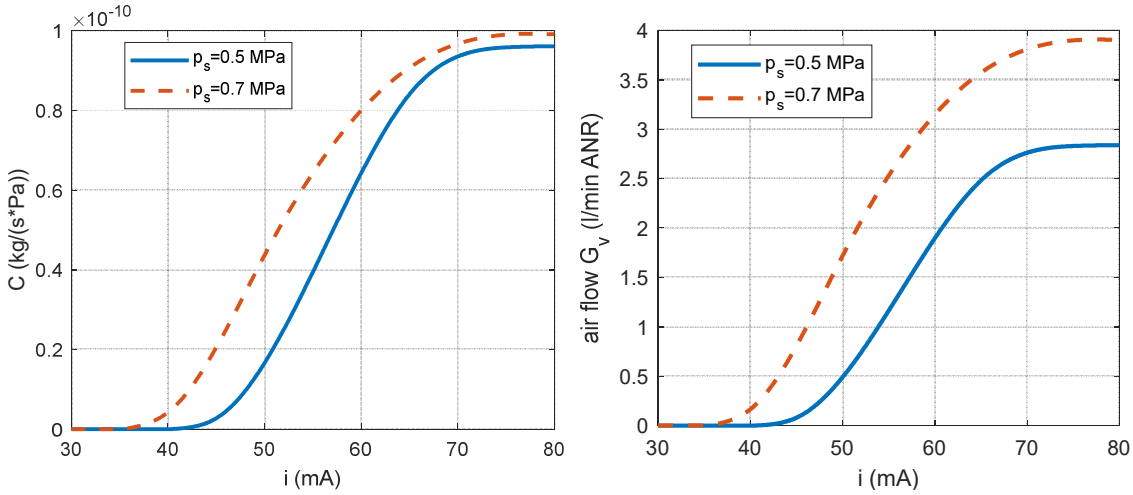

Figure 14: Conductance and air flow through the valve vs input current i with p_s=0.5 and 0.7 MPa

The air flow in sonic conditions ($P<bP_s$) is given by:

$$G_v = C_{st} P_s \tag{13}$$

where b is the critical ratio, P_s the absolute supply pressure and P the absolute downstream pressure.

The air flow in subsonic conditions ($bP_s<P<P_s$) is:

$$G_v = C_{st} P_s \sqrt{1 - \left(\frac{\frac{P}{P_s} - b}{1 - b} \right)^2} \tag{14}$$

Figure 15 plots the flow through the valve vs the downstream pressure P with p_s=0.5 MPa. The sonic region is characterised by constant flow, while the subsonic region is described by an elliptical curve.

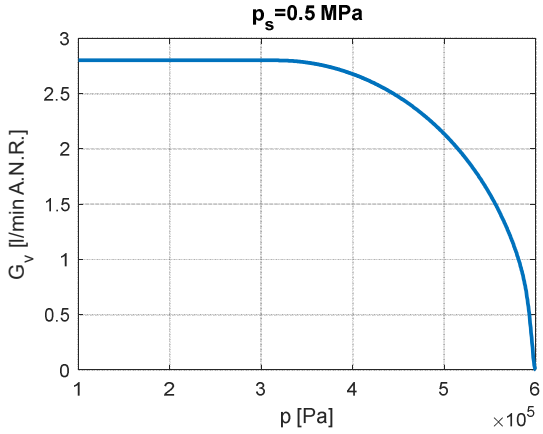

Figure 15: Air flow through the valve vs the downstream absolute pressure P with p_s=0.5 MPa

3.3.2. Dynamic model of the valve

The opening/closing transient of the valve due to an input current step can be modeled with a second-order transfer function:

$$\frac{C(s)}{i(s)} = \frac{K_v}{\frac{s^2}{\omega_n^2} + \frac{2\xi}{\omega_n}s + 1} \tag{15}$$

The conductance is saturated at the maximum value of $10 \cdot 10^{-11}$ kg/(sPa). The response to a current step of 60 mA with p_s=0.5 MPa is depicted in Figure 16.

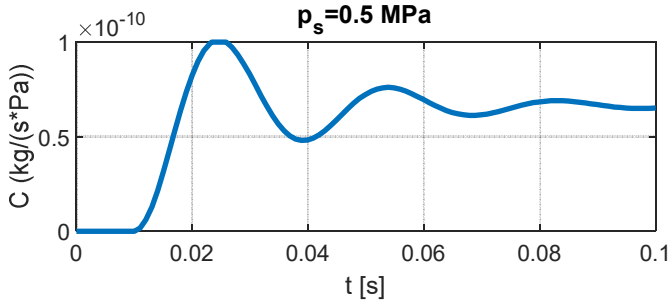

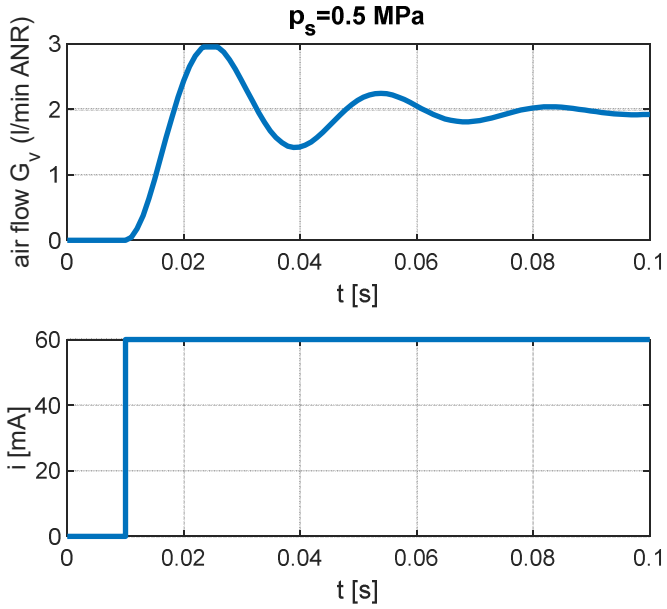

Figure 16: Valve response to a step in input current with p_s=0.5 MPa

4 COMPARISON WITH EXPERIMENTAL DATA

4.1 Tests on the valve alone

The valve is tested with a given gauge supply pressure (p_s=0.5 and 0.7 MPa) and ambient pressure at the output port. The experimental air flow is compared with the simulated one at different input currents in Figure 17. The model is in good accordance with the experimental data.

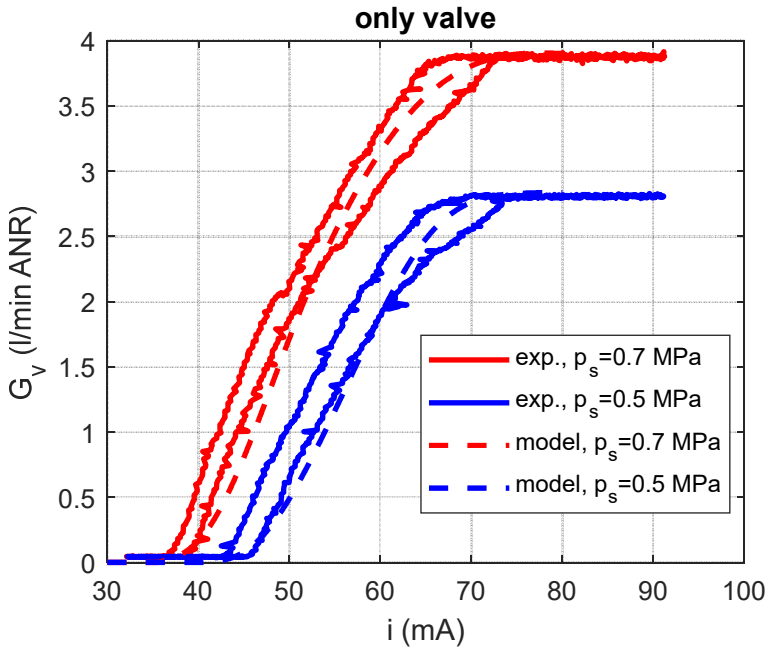

Figure 17: Air flow through the valve vs input current; comparison between experimental and numerical results

4.2 Tests on valve and pad

In Figure 18 the air flow through valve and pad at infinite air gap is plotted vs the input current with valve supplied at p_s=0.5 and 0.7 MPa. The numerical results are compared with experimental ones. The accuracy of the model in this case is lower as the valve model was identified on the base of the experimental tests carried out on the valve alone. The conductance curve depends also on the downstream pressure, which in this case is higher than ambient.

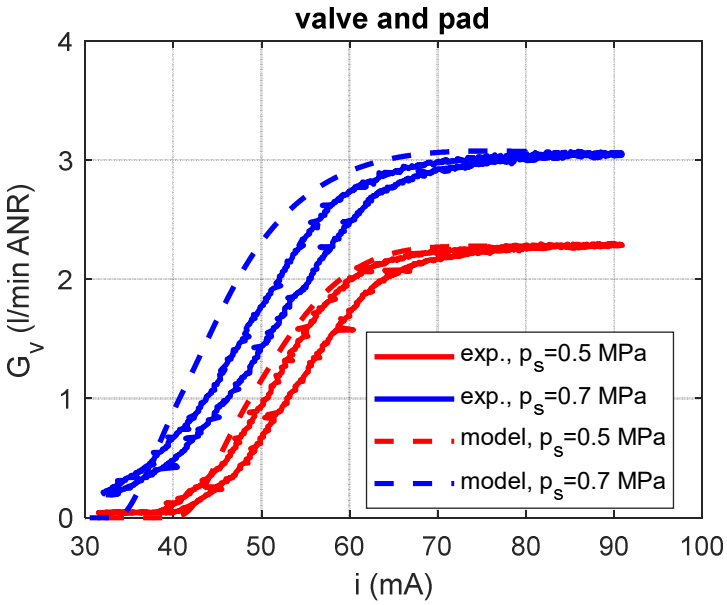

Figure 18: Air flow through the pad in open loop vs input current; comparison between experimental and numerical results

5 CONCLUSIONS AND FUTURE WORK

A new prototype of active aerostatic bearing has been designed and realized. The proportional valve has been modeled considering a non-linear conductance with a dead band dependent on the supply pressure. The pad has been modeled with a simple lumped parameters model able to predict the static characteristics of a generic bearing after validation. Experimental tests have been carried out on the valve alone in order to validate its model; a test bench has been set up in order to test the pad in static conditions.

Future work will concern extensive experimental tests on the passive pad for validation of its model and verification of the model in case of active pad.

REFERENCES

[1] M. R. Bryant, A. E. Velinsky, N. H. Beachley, and F. J. Fronczak, A Design Methodology for Obtaining Infinite Stiffness in Aerostatic Thrust Bearing. *ASME Journal of Mechanical Design*, **108**, 448–453, 1986.

[2] P. L. Holster, J. A. H. Jacobs, Theoretical Analysis and Experimental Verification on the Static Properties of Externally Pressurized Air-Bearing Thrust Bearings with Load Compensation. *Tribology International*, **20**, 276–289, 1987.
[3] K. Sato, K. Yamada, S. Togo, Y. Saito, and K. Unno, Study on Externally Pressurized Gas Bearings with Infinite Stiffness (2nd Report) - Experiments on the Static Characteristics of a Circular Thrust Bearing. *Journal of the Japan Society for Precision Engineering*, **62**(1), 85–89, 1996.
[4] M. F. Chenn, Y. T. Lin, Dynamic Analysis of the X-Shaped Groove Aerostatic Bearings with Disk–Spring Compensator. *JSME International Journal - Series C: Mechanical Systems Machine Elements and Manufacturing Quarterly*, **45**, 492–501, 2002.
[5] K. Y. Huang, Y. C. Shiao, Design and Development of Magneto-strictive Actuating Restrictor for Aerostatic Thrust Bearing. *Proceedings of the 12th IFToMM World Congress*, Besancon, France, June 17–20, 2007.
[6] S. K. Ro, S. Kim, Y. Kwak, and C. H. Park, A Linear Air Bearing Stage with Active Magnetic Preloads for Ultraprecise Straight Motion. *Precision Engineering*, **34**, 186–194, 2010.
[7] H. Mizumoto, S. Arii, Y. Kamit, K. Goto, T. Yamamoto, and M. Kawamoto, Active Inherent Restrictor for Air-Bearing Spindles. *Precision Engineering*, **19**, 141–147, 1996.
[8] G. Aguirre, F. Al-Bender, and H. Van Brussel, Dynamic Stiffness Compensation with Active Aerostatic Thrust Bearings. *Proceedings of ISMA2008*, Leuven, Belgium, September 15–17, 2008.
[9] F. Al-Bender, H. Van Brussel, Active Dynamic Compensation of Aerostatic Bearings. *Proceedings of the International Conference on Noise and Vibration Engineering. International Conference on Noise and Vibration Engineering*, Leuven, Belgium, 1994.
[10] G. Belforte, T. Raparelli, V. Viktorov, and A. Trivella, Analysis of Steady and Transient Characteristics of Pneumatic Controlled Air Bearing. *Proceedings of the 5th JFPS International Symposium on Fluid Power*, Nara, Japan, November 12–15, 2002.
[11] G. Belforte, and T. Raparelli, Development of a New Actively Compensated Pneumatic Journal Bearing. *Proceedings of 4th Scandinavian International Conference on Fluid Power*, Tampere, Finland, September 26–29, 1995.
[12] T. Raparelli, V. Viktorov, F. Colombo, and L. Lentini, Aerostatic Thrust Bearings Active Compensation: Critical Review. *Precision Engineering*, **44**, 1–12, 2015.
[13] D. Maffiodo, F. Colombo, T. Raparelli, Open and closed loop control of an active air bearing with digital valves. *AIMETA 2017 - Proceedings of the 23rd Conference of the Italian Association of Theoretical and Applied Mechanics*, **4**, 641-649, 2017.
[14] F. Colombo, D. Maffiodo, T. Raparelli, Active Gas Thrust Bearing With Embedded Digital Valves and Backpressure Sensors. *Tribology Transactions*, **60**(5), 807-813, 2017. DOI: 10.1080/10402004.2016.1213344.
[15] D. Maffiodo, F. Colombo, T. Raparelli, Numerical model of digital valve-controlled active air bearing. *International Journal of Automation Technology*, **13**(1), 141-148, 2019. DOI: 10.20965/IJAT.2019.P0141.